Adsorption of xenon and CH_4 mixtures in zeolite NaA. ^{129}Xe NMR and grand canonical Monte Carlo simulations

Cynthia J. Jameson
Department of Chemistry M/C-111, University of Illinois at Chicago, 845 W. Taylor, Chicago, Illinois 60607-7061

A. Keith Jameson
Department of Chemistry, Loyola University, Chicago, Illinois 60626

Pavel Kostikin and Bernoli I. Baello
Department of Chemistry M/C-111, University of Illinois at Chicago, 845 W. Taylor, Chicago, Illinois 60607-7061

(Received 17 March 1999; accepted 1 October 1999)

Investigation of competitive adsorption is carried out using the Xe–CH_4 mixture in zeolite Na*A* as a model system. The Xe_n clusters are trapped in the alpha cages of this zeolite for times sufficiently long that it is possible to observe individual peaks in the NMR spectrum for each cluster while the CH_4 molecules are in fast exchange between the cages and also with the gas outside. The ^{129}Xe nuclear magnetic resonance spectra of nine samples of varying Xe and CH_4 loadings have been observed and analyzed to obtain the ^{129}Xe chemical shifts and the intensities of the peaks which are dependent on the average methane and xenon occupancies. The distributions P_n, the fraction of cages containing *n* Xe atoms, regardless of the number of CH_4 molecules are obtained directly from the relative intensities of the Xe_n peaks. From the observed ^{129}Xe chemical shift of each Xe_n peak can be obtained the average number of CH_4 molecules in the same cavity as *n* Xe atoms. Grand canonical Monte Carlo (GCMC) simulations of mixtures of Xe and CH_4 in a rigid zeolite Na*A* lattice provide the detailed distributions and the average cluster shifts, as well as the distributions P_n. The agreement with experiment is reasonably good for all nine samples. The calculated absolute chemical shifts for the Xe_n peaks in all samples at 300 K range from 80 to 230 ppm and are in good agreement with experiment. We also consider a very simple strictly statistical model of a binary mixture, derived from the hypergeometric distribution, in which the component molecules are distinguishable but equivalent in competition for eight lattice sites per cage under mutual exclusion. The latter simple model provides a limiting case for the distributions, with which both the GCMC simulations and the properties of the actual Xe–CH_4 system are compared. The ideal adsorbed solution theory gives a first approximation to the selectivity of the adsorption of the Xe and CH_4 from a mixture of gases, but starts to fail at high total pressures, especially at low CH_4 mole fraction in the bulk. © *2000 American Institute of Physics.* [S0021-9606(90)70201-2]

INTRODUCTION

Industrial adsorption processes generally involve adsorption of multicomponent mixtures. The distribution and dynamic behavior of a binary mixture of adsorbed species in a microporous material is of significant interest for heterogenous catalytic processes and separations applications of these materials.[1] Adsorption and diffusion of mixtures in zeolites are found to be strongly dependent on the composition of the fluid phase.[2] For the *A*-type zeolites, Na*A*, K*A*, and Ag*A*, for example, it has been found that the measurement of the distribution of molecules among the cages and the rate constants for cage-to-cage migration of pure xenon can be carried out using ^{129}Xe nuclear magnetic resonance,[3–8] and the experimental data (adsorption isotherms, distributions, and chemical shifts in a sample of adsorbed xenon in equilibrium with the bulk phase) can be reproduced satisfactorily by employing grand canonical Monte Carlo methods in the averaging.[7,9–11] For binary mixtures of Xe and CH_4 in zeolite Na*A*, we adopt the following strategy: Calculate the theoretical shielding functions of ^{129}Xe in Xe–CH_4; test the function against chemical shift measurements in gas phase mixtures using available anisotropic potential surfaces for the Xe–CH_4 interaction. Adopt a CH_4–CH_4 interaction potential function and a CH_4-zeolite potential function. Test these against the temperature dependent adsorption isotherms of pure CH_4 in zeolite Na*A* by doing GCMC simulations of CH_4 in Na*A*. Then use GCMC simulations of Xe–CH_4 mixtures in the zeolite to obtain distributions and mixture adsorption isotherms, to be compared with ideal adsorbed solution theory. Finally, GCMC simulations on equilibrium bulk phase/adsorbed phase Xe–CH_4/Na*A* systems that match the composition of the experimental samples will generate distributions and chemical shifts that can be compared against the experimental values of about 5–6 intensities and the corresponding chemical shifts in each of nine samples. In principle, there is sufficient detail in these experiments for stringent tests of the simulations. If the simulations can reproduce the experimental val-

ues satisfactorily, then we may derive from the GCMC simulations more detailed pictures (one-body distribution functions, two-body distribution functions, etc.) of the behavior of Xe and CH_4 in competitive adsorption in a zeolite.

EXPERIMENTS

Sample preparation has been previously described.[4] Four mm (o.d.) tubes are fashioned from ordinary borosilicate tubing, containing a volume of 0.20–0.25 mL, calibrated with mercury. A known mass of zeolite is introduced (typically 50 mg), dried for 16 h under ''thin-bed'' conditions at 350–400 °C under vacuum. A known number of moles of Xe and CH_4 are introduced and the sample is flame-sealed under liquid nitrogen. The mass balance of Xe and CH_4 between the adsorbed and gaseous phases can be obtained from NMR data in an experimental manner.

^{129}Xe spectra were taken on Bruker AC-200, Varian VXR-300S and Bruker AM-400 spectrometers, temperature-controlled to within about 0.2 K at 300 K using the ^{1}H spectrum of neat ethylene glycol. The experimental relaxation times of all Xe_n clusters in a given sample are identical due to cage-to-cage migration. Thus, the relative peak intensities of Xe_n in these specific systems are reliable over a wide range of recycle times. 4 K data points were collected for all spectra with 2000–20 000 transients being averaged in each case. Spectra were taken with the spectrometer unlocked (magnetic field drift is negligible), B_0 being reproducibly set by setting the methylene proton of ethylene glycol to a predetermined resonance frequency.

COMPUTATIONAL METHODS

The grand canonical ensemble is appropriate for adsorption systems, in which the adsorbed phase is in equilibrium with the gas at some specified temperature. The use of a computer simulation allows us to calculate average macroscopic properties directly without having to explicitly calculate the partition function. The grand canonical Monte Carlo (GCMC) method as applied in this work has been described in detail earlier.[9,10] The potential functions and the shielding functions are cut-and-shifted to be consistent with the use of the minimum image convention[12] in the periodic boundary conditions. The effective potentials describing the interaction between the adsorbed molecules and the zeolite, the Xe–Xe, and Xe–CH_4 potential functions, and the Xe–CH_4 shielding function used are the ones described below. The simulation box is a unit cell of zeolite Na*A*, with the atomic coordinates, including the Na cations, taken from the x-ray single crystal refinement of the dehydrated zeolite by Pluth and Smith.[13] This is unchanged from our previous work.[9] The Markov chain is constructed using the Norman–Filinov method, that is, using three equally weighted types of moves, one involving displacement of a particle, and two moves randomly chosen from destruction or creation of a particle,[14] as in our previous work.[9] The core of the program effects the creation/destruction and displacement of one molecule at a time and calculates the associated energy change, ΔU in each case. This is used to continuously update the total configurational energy of the system, without having to recalculate every interaction at every step. The displacement step uses the adsorbed phase composition in the choice of either fluid. The creation/destruction step begins with the decision to either create or destroy a particle. If the decision is to destroy a particle (that is, the particle is assumed to go into the gas phase) the choice between destroying an atom of Xe or CH_4 is made proportionately to the gas phase composition, i.e., ρ_{Xe} and ρ_{CH_4}. The choice of creating an atom of Xe or CH_4 is likewise made according to the gas phase composition. The chemical potential of the Xe and the CH_4 appropriate to the temperature and densities in the gas mixture, using the virial coefficients, are

$$\mu_1-\mu_1^0=2RT(\rho_1B_{11}+\rho_2B_{12})+RT\ln(\rho_1/\rho^0), \tag{1a}$$

$$\mu_2-\mu_2^0=2RT(\rho_2B_{22}+\rho_1B_{12})+RT\ln(\rho_2/\rho^0). \tag{1b}$$

These chemical potentials for the adsorbed phase with which the gas mixture is in equilibrium, the temperature, and the mole fraction of CH_4 in the gas are the parameters of a GCMC simulation.

The added complication of a sorbate with structure is that the orientation of the CH_4 has to be generated at each displacement or creation step. This is easily done since we are using sorbate molecules with rigid geometry. In a displacement step for CH_4 a random orientation is also chosen before it is accepted from the same probability distribution. The orientation of a rigid body specifies the relation between an axis system fixed in space and one with respect to the body. A unit vector in the body-fixed frame $\mathbf{e_b}$ can be obtained by

$$\mathbf{e_b}=\mathbf{A}\cdot\mathbf{e_s}$$

from the unit vector $\mathbf{e_s}$ in the space fixed frame. Any orientation is defined as a series of rotations about the body-fixed axes, an anticlockwise rotation ϕ, (0 to 2π) about the z axis; an anticlockwise rotation θ (0 to π) about the x axis, and an anticlockwise rotation ψ (0 to 2π) about the z axis. The rotation matrix $\mathbf{A}$ is

$$\mathbf{A}=\begin{bmatrix} \cos\psi\cos\phi-\cos\theta\sin\phi\sin\psi & \cos\psi\sin\phi+\cos\theta\cos\phi\sin\psi & \sin\psi\sin\theta \\ -\sin\psi\cos\phi-\cos\theta\sin\phi\cos\psi & -\sin\psi\sin\phi+\cos\theta\cos\phi\cos\psi & \cos\psi\sin\theta \\ \sin\theta\sin\phi & -\sin\theta\cos\phi & \cos\theta \end{bmatrix}.$$

TABLE I. Potential function parameters used in this work for sorbate interactions.

	γ	m	$r_{\min}$, Å	ε/k_B, K
$V(r_{Xe-Xe})$	11	13	4.3627	282.29
$V(r_{Xe-C})$	9.5	13	4.0047	141.52
$V(r_{Xe-H})$	9.5	13	3.671	53.07
$V(r_{C-C})$	8	11.5	3.915	230.1
	A, K	b, Å^{-1}		
$V(r_{H-H})$	4.2308×10^5	3.77		

The position of the hydrogen atoms are expressed as unit vectors relative to the central carbon atom for an arbitrarily chosen body-fixed frame $\mathbf{e_b}$. A new orientation in the space fixed frame is made by choosing three random numbers, generated from a uniform distribution on (0, 1) to represent cos θ, ϕ, and ψ, normalized, respectively, to the range -1 to $+1$, 0 to 2π and 0 to 2π, respectively. The transpose of the rotation matrix is then calculated and applied to $\mathbf{e_b}$.[15] Alternative methods are given in Ref. 12.

In our approach, the ^{129}Xe shielding, like the energy, is taken to be expressible as a sum of pairwise contributions, using atom–atom shielding functions that are likewise cut and shifted. The Xe–O and Xe–Na shielding functions used here are the same as was used in our previous work.[9,10,16] The new Xe–CH_4 shielding function is as described below.

THE POTENTIAL FUNCTIONS, V(Xe–Xe), V(Xe–CH_4), AND V(CH_4–CH_4)

The Xe–Xe potential function used is the best two-body potential of Aziz and Slaman,[17] fitted to the form suggested by Maitland and Smith:[18]

$$V(\mathrm{Xe\text{–}Xe}) = \varepsilon\left\{\frac{6}{n-6}\overline{r}^{-n} - \frac{n}{n-6}\overline{r}^{-6}\right\}, \tag{2}$$

where n is allowed to vary with $\overline{r} = r/r_{\min}$ according to $n = m + \gamma(\overline{r} - 1)$. This is the same Xe–Xe potential we have used throughout our work on Xe in zeolites,[7,9–11,19] and the parameters are given in Table I.

The CH_4–CH_4 interaction potential is taken from the potential of Righini, Maki, and Klein[20] (RMK) which had been fitted to the second pressure virial coefficients $B_{11}(T)$ of CH_4 at 100–600 K, and the thermodynamic properties of solid methane, including the low temperature phase transitions. Meinander and Tabisz[21] examined the effect of the anisotropy of the potential on the second virial coefficient and found that the RMK potential is a very good representation of the intermolecular potential of CH_4 and superior to previously proposed functions. The RMK function is

$$V(\mathrm{CH_4\text{–}CH_4}) = V(r_{C-C}) + \sum_i \sum_j V(r_{H_i-H_j}), \tag{3}$$

where $V(r_{H-H})$ is of the form $A\exp[-br_{H-H}]$. We have used $V(r_{H-H})$ unchanged, but $V(r_{C-C})$ is modified slightly to be of the Maitland–Smith form rather than the original Hartree–Fock damped form of the RMK potential. The parameters of the potential functions used in this work are given in Table I. The form we have used reproduces the pure CH_4 second virial coefficients calculated by the RMK function. Other potential functions that had been used in the literature are of the form

$$V(\mathrm{CH_4\text{–}CH_4}) = V_{LJ}(r_{C-C}) + \sum_p \sum_j V_{LJ}(r_{C_p-H_j}) + \sum_i \sum_j V_{LJ}(r_{H_i-H_j}) \tag{4}$$

with various parameters.[22,23] They do not reproduce the experimental $B_{11}(T)$ of CH_4 as well as the RMK potential does, in one case it is clear that the potential function had never been tested against the virial coefficient.[23]

The Xe–CH_4 interaction potential used in this work is based on the isotropic potential function of Liuti *et al.*[24] which had an MSV form (Morse-spline–van der Waals) and had been parametrized to reproduce the absolute values of the integral cross sections and the glory extrema positions from molecular beam scattering experiments. We fitted the Liuti potential function using the site–site form,

$$V(\mathrm{Xe\text{–}CH_4}) = V(r_{Xe-C}) + \sum_i V(r_{Xe-H_i}) \tag{5}$$

where $V(r_{Xe-C})$ and $V(r_{Xe-H_i})$ are taken to be of the Maitland–Smith form with the parameters given in Table I. Since the shielding functions go to large negative values at close approach, it is quite important to have Xe–Xe and Xe–CH_4 potentials that have the correct behavior at these short distances, especially close to r_0. The Maitland–Smith form provides a superior fit to the best Aziz potential for Xe–Xe and to the MSV form of the Xe–CH_4 potential of Liuti *et al.*, and is just as inexpensive as the Lennard-Jones form in computational overhead. The initial V(Xe–C) parameters used in the iterative fitting procedure were obtained by applying combining rules starting from the V(Xe–Xe) and V(CH_4–CH_4). The resulting Xe–CH_4 potential function in Eq. (5) was tested against the mixed second pressure virial coefficients $B_{12}(T)$ measured by Brewer.[25] In addition it was found to reproduce the correlating equation found by Brewer for the mixed second virial of Xe–CH_4.[25] Thus, we believe the potential function described by Eq. (5) with parameters given in Table I, obtained by fitting to the Liuti *et al.* potential, is adequate to describe the Xe–CH_4 interactions in the gas phase mixture with respect to pressure behavior and chemical potentials. This potential function was also found to be adequate to reproduce the second virial coefficient of the ^{129}Xe chemical shift due to interaction with the CH_4 molecule, as described below.

THE SHIELDING FUNCTION, σ(^{129}Xe, Xe–CH_4)

The values of the ^{129}Xe shielding function were obtained for various Xe-*C* distances at three different orientations of the CH_4: with the Xe-*C* distance vector placed along an H-C bond, along a bisector of the H-C-H angle, and along a normal to the equilateral triangle of three H atoms. Initially the ^{39}Ar shielding was calculated for the Ar–CH_4 system at these orientations, using both the LORG method of Hansen and Bouman[26] and the GIAO method of Wolinski and

Pulay[27] with full counterpoise corrections at each of the 96 configurations of the pair. It is interesting to note that using the same basis set, the counterpoise corrections were larger in the GIAO method than in the LORG method. The scaling of the shielding of ^{39}Ar in the Ar–CH_4 system to the ^{129}Xe shielding in the Xe–CH_4 system were carried out at each configuration by using the factors

$$\frac{\alpha_{\mathrm{Xe}}}{\alpha_{\mathrm{Ar}}}\times\frac{\langle a_0^3/r^3\rangle_{\mathrm{Xe}}}{\langle a_0^3/r^3\rangle_{\mathrm{Ar}}}\times\frac{U_{\mathrm{Xe}}(U_{\mathrm{Ar}}+U_{\mathrm{CH_4}})}{U_{\mathrm{Ar}}(U_{\mathrm{Xe}}+U_{\mathrm{CH_4}})}$$

for the ^{129}Xe shielding, and the factor

$$\frac{r_0(\mathrm{Xe-CH_4})}{r_0(\mathrm{Ar-CH_4})}$$

for the Xe–C distance. The fundamental properties (α, $\langle a_0/r^3\rangle$, and ionization potential U) of Xe, Ar, and CH_4 were taken from Refs. 28, 29, and 30, respectively. The r_0 of the best isotropic potentials for Xe–CH_4 (Righini *et al.*, Ref. 20) and Ar–CH_4 (Buck *et al.*, Ref. 31) were used in the scaling of the distance between the centers. No adjustable parameters were used in the scaling. The resulting ^{129}Xe–CH_4 shielding values at 96 configurations are then represented by a functional form, for use in obtaining average chemical shifts for the gas phase and for the simulations of the Xe–CH_4 mixture inside the zeolite. The ^{129}Xe shielding function for the Xe–CH_4 system is written as

$$\sigma(^{129}\mathrm{Xe},\mathrm{Xe-CH_4})=\sigma(^{129}\mathrm{Xe},r_{\mathrm{Xe-C}})+\sum_i\sigma(^{129}\mathrm{Xe},r_{\mathrm{Xe-H_i}}). \quad (6)$$

The individual functions are of the form

$$\sigma(^{129}\mathrm{Xe},r)=a_6r^{-6}+a_8r^{-8}+a_{10}r^{-10}+a_{12}r^{-12}+a_{14}r^{-14}, \quad (7)$$

where $r=r_{\mathrm{Xe-C}}$ or $r_{\mathrm{Xe-H_i}}$. The coefficients were found by least squares fitting to the 96 calculated $\sigma(^{129}\mathrm{Xe},\mathrm{Xe-CH_4})$ values.

The ^{129}Xe shielding function for the Xe–CH_4 system was tested against the experimental density coefficient of the ^{129}Xe chemical shift in gaseous mixtures of Xe and CH_4.[32] In such mixtures, the shielding is represented by an expansion in the densities

$$\sigma(T,\rho_{\mathrm{Xe}},\rho_{\mathrm{CH_4}})=\sigma_0+\sigma_1(T)_{\mathrm{Xe-Xe}}\rho_{\mathrm{Xe}}+\sigma_1(T)_{\mathrm{Xe-CH_4}}\rho_{\mathrm{CH_4}}+\cdots, \quad (8)$$

where σ_0 is the shielding of an isolated Xe atom, and the densities in pure Xe samples and the samples of Xe–CH_4 mixtures are used to determine the second virial coefficients $\sigma_1(T)_{\mathrm{Xe-Xe}}$ and $\sigma_1(T)_{\mathrm{Xe-CH_4}}$.[32] The values of $\sigma_1(T)_{\mathrm{Xe-CH_4}}$ are given by the integral

$$\sigma_1(T)_{\mathrm{Xe-CH_4}}=\int\int\int\int\{\sigma(^{129}\mathrm{Xe},\mathrm{Xe-CH_4}(r,\theta,\phi,\psi))-\sigma_0\}\times\exp[-V(r,\theta,\phi,\psi)/k_BT]. \quad (9)$$

The values of this integral are shown in Fig. 1 in comparison with the experimental data in the range 230–440 K. First of all, the sign is correct. Second, the order of magnitude of the values at room temperature and above is remarkably close to experiment. Third, the qualitative change with temperature is the same as in experiment. The agreement is very good except at the lowest temperatures. We had found deviations to be in the same direction for the Xe–Xe, Xe–Kr, Xe–Ar pairs as well; i.e., the absolute magnitudes of the experimental values are larger than the values obtained from integrating over the *ab initio* shielding functions at the lowest temperatures.[33]

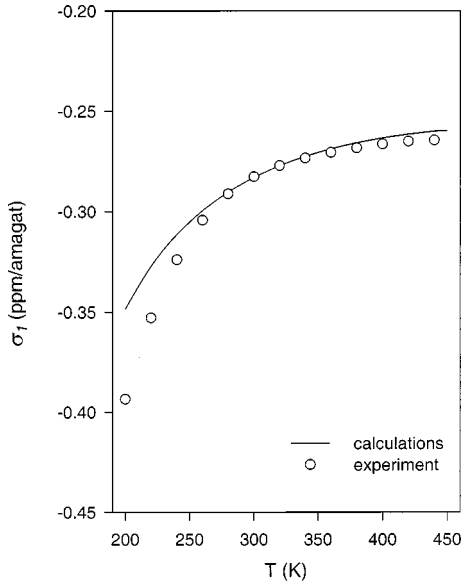

FIG. 1. Second virial coefficient of the ^{129}Xe nuclear shielding calculated from the Xe–CH_4 shielding function given by Eq. (6) and the V(Xe–CH_4) given by Eq. (5) is compared with the experimental values obtained from the ^{129}Xe chemical shift in gas phase mixtures of Xe and CH_4.

For Xe–CH_4 mixtures in the zeolite the average chemical shifts are calculated using the Metropolis Monte Carlo method. At given chemical potentials,

$$\sigma(\mu_{\mathrm{Xe}},\mu_{\mathrm{CH_4}},T,V)=(1/M)\sum_{i=1}^{M}\sigma_i(\mathbf{r}^n), \quad (10)$$

where the configurations $i=1$ to M are generated by a Markov chain constructed so that its limiting distribution is the required probability distribution for a grand canonical ensemble. In GCMC the Markov chain is constructed so that the limiting distribution is proportional to

$$\exp\{-[U(\mathbf{r}^N)-N\mu]/k_BT-\ln N!-3N\ln(h^2/2\pi mk_BT)^{1/2}+N\ln V\}.$$

The function $\sigma_i(\mathbf{r}^N)=\sigma(\mathbf{r}_1,\mathbf{r}_2,\mathbf{r}_3,\mathbf{r}_4,\ldots)$ is the pairwise additive shielding function, summed over all the Xe–O, Xe–Na^+, Xe–Xe, Xe–C, and Xe–H distances in the ith configuration. Likewise $U(\mathbf{r}^N)$ is the (in this work, pairwise additive) interaction potential function.

THE INTERACTION POTENTIAL BETWEEN THE SORBATES AND THE ZEOLITE

Before we can carry out the grand canonical Monte Carlo averaging of the distributions and the chemical shifts

TABLE II. Lennard-Jones parameters used for the effective pairwise potentials that are used here to model the sorbate–zeolite interaction.

	r_0, Å	ϵ/k_B, K
$V(\mathrm{Xe–O_{zeol}})$	3.37	217.0
$V(\mathrm{Xe–Na^+_{zeol}})$	3.676	39.08
$V(\mathrm{C–O_{zeol}})$	2.843	109.2
$V(\mathrm{C–Na^+_{zeol}})$	3.225	16.62
$V(\mathrm{H}_i\mathrm{–O_{zeol}})$	2.358	113.6
$V(\mathrm{H}_i\mathrm{–Na^+_{zeol}})$	2.713	14.31

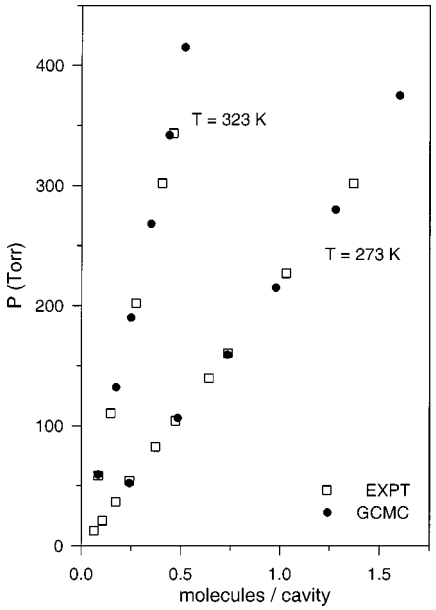

FIG. 2. Adsorption isotherms from GCMC simulations of pure CH_4 in zeolite Na*A* at 273 and 323 K are compared with the experimental data of Ruthven (Ref. 43).

of the mixture of Xe and CH_4 in the zeolite Na*A*, we need to test the interaction potentials V(Xe–zeolite) and $V(CH_4$–zeolite) against the known properties of both the pure Xe in the zeolite and of pure CH_4 in the zeolite. Although we have also carried out simulations explicitly including the inductive interactions between Xe and the zeolite,[19,34] we do not do that here. Instead, we use the same V(Xe–zeolite) that we have used previously for pure xenon in Na*A*,[9] and for mixtures of rare gases in Na*A*.[10,16] where the entire interaction is represented by an effective potential that is of the form

$$V(\mathrm{Xe–zeolite}) = \sum V_{\mathrm{LJ}}(\mathrm{Xe–O_{zeol}}) + \sum V_{\mathrm{LJ}}(\mathrm{Xe–Na^+_{zeol}}), \tag{11}$$

using the same Lennard-Jones parameters as we have used before, shown in Table II. For the pure CH_4 in zeolite Na*A*, we use the same effective potential function used by Woods and Rowlinson for CH_4 in Na*X*,[35] summing over the O atoms of the zeolite framework and the Na^+ counterions:

$$V(\mathrm{CH_4–zeolite}) = \sum V_{\mathrm{LJ}}(\mathrm{C–O_{zeol}}) + \sum V_{\mathrm{LJ}}(\mathrm{C–Na^+_{zeol}}) + \sum_i \left\{ \sum V_{\mathrm{LJ}}(\mathrm{H}_i\mathrm{–O_{zeol}}) + \sum V_{\mathrm{LJ}}(\mathrm{H_i–Na^+_{zeol}}) \right\}. \tag{12}$$

The parameters of this potential function are summarized in Table II. An alternative set of effective Lennard-Jones functions have been used by Maddox and Rowlinson for CH_4 in Na*Y*,[36,37] and by June *et al.*[38] for CH_4 in silicalite. There are other potential parameters that had been used for CH_4 in Na*A* in models which explicitly include induction terms using partial charges on the oxygen and Na,[39–41] and a more complete description of the interactions between sorbate and zeolite uses distributed multipoles,[42] but we opted for a simple description [Eq. (12)] that does not introduce a large number of parameters. The ability of the adopted potential to reproduce the adsorption isotherm of pure CH_4 in Na*A* is an important one for this work because the loading of CH_4 at a given overhead pressure and bulk composition determines the average number of CH_4 molecules that can provide contributions to the Xe chemical shift. We have to start out with a reasonable description of the CH_4 loading in Na*A* in the absence of Xe, if we expect to represent the competitive distribution of CH_4 and Xe among the cages.

The effective sorbate–zeolite potentials were tested against the adsorption isotherms of the pure components, Xe in zeolite Na*A* and CH_4 in zeolite Na*A*. The experimental adsorption isotherm data of Xe in Na*A* were reported in Ref. 9 and the comparison with simulations were shown there. For CH_4 there are adsorption isotherms from Yucel and Ruthven,[43] and some older data from Harper *et al.*[44] In connection with other experiments, we also have measured (by NMR spectroscopy) the adsorption isotherms of CD_4 in Na*A* at 262.9 K, 301.6 K, 329.5 K, and 361.5 K for loadings up to about 5 CD_4 per cage. Agreement is good between Ruthven's data and ours. We show in Fig. 2 the comparison of the calculated adsorption isotherms from our simulations with Ruthven's experiments at 273 and 323 K. The agreement of the adsorption isotherms from the GCMC simulation of pure CH_4 in Na*A* with experimental data is good when we use the modified RMK potential for $V(CH_4–CH_4)$ shown in Eq. (3) and Table I, and the Woods potential parameters[35] for $V(CH_4$–zeolite) shown in Eq. (12) and Table II. The other CH_4–zeolite potentials did not do as well. Therefore, we choose the Woods potential parameters for the work described below.

Having tested the $CH_4–CH_4$ and the $Xe–CH_4$ potential functions against pressure virial coefficients and other properties, and having tested the $Xe–CH_4$ shielding function and $Xe–CH_4$ potential against the density coefficient of the Xe chemical shift in gas mixtures of Xe and CH_4, and also having tested the CH_4 zeolite interactions against the experimental adsorption isotherms for pure CH_4 adsorption in zeolite Na*A*, we are now ready to consider the results for mixtures of Xe and CH_4 in zeolite Na*A*. The results of the GCMC simulations are analyzed to provide the usual one-body distribution functions, pair distribution functions, and occupan-

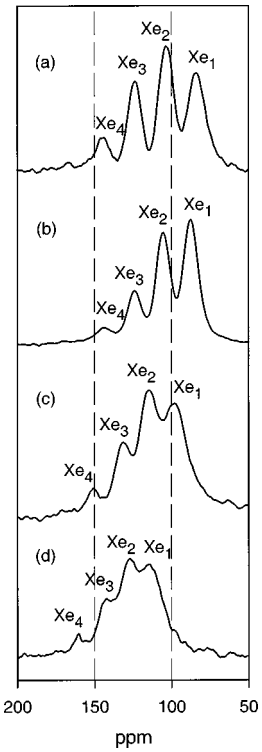

FIG. 3. Typical ^{129}Xe NMR spectra of mixtures of Xe and CH_4 at equilibrium in dehydrated zeolite Na*A*, with increasing loading of CH_4 from top to bottom. The Xe and CH_4 loadings in these samples are (a) $\langle n\rangle_{Xe}=1.250$, $\langle m\rangle_{CH_4}=0.915$; (b) $\langle n\rangle_{Xe}=0.888$, $\langle m\rangle_{CH_4}=1.509$; (c) $\langle n\rangle_{Xe}=1.056$, $\langle m\rangle_{CH_4}=2.208$; (d) $\langle n\rangle_{Xe}=1.046$, $\langle m\rangle_{CH_4}=3.860$.

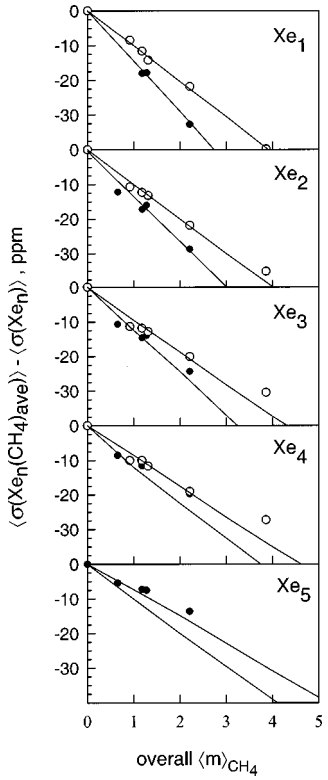

FIG. 4. Experimental ^{129}Xe chemical shifts of Xe_n, $\{\langle\sigma(Xe_nCH_{4ave})\rangle - \langle\sigma(Xe_n)\rangle\}$, for $n=1$ to 5 in mixtures of Xe and CH_4 in zeolite Na*A* for $\langle n\rangle_{Xe}=0.89-1.59$(○) and for $\langle n\rangle_{Xe}=2.786-3.89$(●). The average Xe_n chemical shift increments $\{\langle\sigma[Xe_n(CH_4)_{ave}]\rangle - \langle\sigma[Xe_n]\rangle\}$, predicted by the hypergeometric distribution for $\langle n\rangle_{Xe}=1.25$ and 3.30 in mixtures of Xe and CH_4 in zeolite Na*A* are shown as lines.

cies. In addition, the average shieldings for individual mixed clusters $Xe_n(CH_4)_m$, which are independent of loading, are accumulated over all the GCMC runs, as well as the averages for Xe_n clusters for each (μ_1,μ_2,T). Calculations reported here were carried out on IBM RISC/6000 (models 560 and 365) and HP Apollo series 700 workstations.

RESULTS AND DISCUSSIONS

Experimental ^{129}Xe chemical shifts and distributions of xenon atoms

In samples of pure Xe in Na*A*, the Xe_n chemical shifts at a given temperature are the same for all samples, independent of loading. Typical ^{129}Xe NMR spectra of Xe–CH_4 mixtures in Na*A* are shown in Fig. 3. The changes in the Xe_n chemical shifts from those found in pure xenon in Na*A* are due to the presence of the other sorbate, in this case, CH_4. The intensities provide directly, of those cages having Xe, the fraction of cages occupied by exactly *n* Xe atoms. The distribution of Xe atoms among all cages, P_n, can be obtained from these. The determination of $\langle n\rangle_{Xe}$ the overall average number of Xe atoms per cage, and $\langle m\rangle_{CH_4}$ the overall average number of CH_4 molecules per cage in a given sample are described in detail in Ref. 10. The incremental chemical shift values for each Xe_n with increasing loading of CH_4 are shown in Fig. 4 for nine samples of Xe–CH_4 mixtures in Na*A*. The most important trend in this figure is that the incremental chemical shift of a particular Xe_n increases with increasing overall CH_4 loading. This increase is more pronounced for the samples with the larger Xe loading (filled circles have $\langle n\rangle_{Xe}=2.8-3.9$, open circles have $\langle n\rangle_{Xe}=0.9-1.6$ Xe per cage). The other striking trend is that the larger the Xe_n cluster, the smaller the dependence of the ^{129}Xe chemical shift on the overall $\langle m\rangle_{CH_4}$. The lines in this figure are related to a simple statistical explanation that will be discussed in a later section.

GCMC simulations

The average ^{129}Xe shielding in $Xe_n(CH_4)_m$

Figure 5 shows how the ^{129}Xe shielding for $Xe_n(CH_4)_m$ in an alpha cage are systematically of greater magnitude than those for the corresponding Xe_nAr_m from the GCMC simulations. That is, the incremental chemical shift upon adding each CH_4 molecule is greater than that of adding each Ar atom to Xe_n, and this difference is more pronounced for the larger *n*. On the other hand, Table III shows that the average shielding of $Xe_n(CH_4)$ is rather similar to, and only slightly less than the corresponding Xe_nKr. In the case of Xe_nKr, the individual peaks have been observed experimentally,[45] whereas peaks for $Xe_n(CH_4)_m$ have not. GCMC simulations similar to those reported here have reproduced the observed chemical shifts of Xe_nKr to within a few ppm (2%).[16] The chemical shifts calculated here for Xe_nCH_4 are expected to be as reliable as those for Xe_nKr.

The ^{129}Xe chemical shifts of the Xe_n clusters in a cage of Na*A*, with or without the coadsorbate molecules, could not

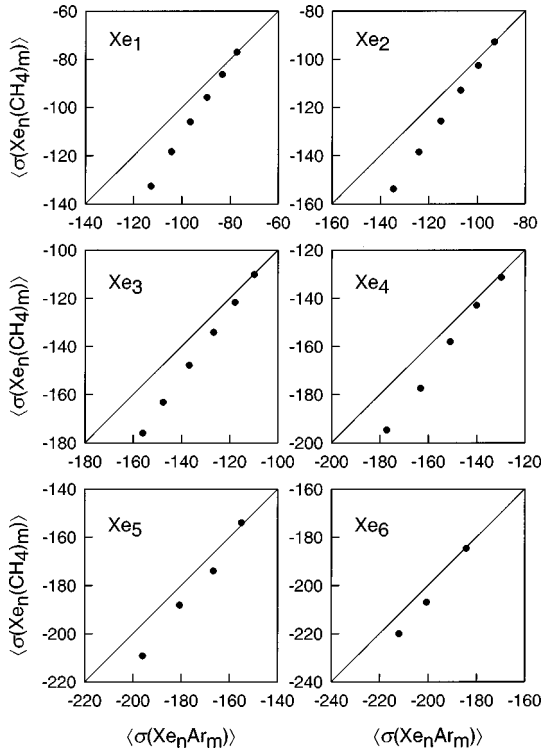

FIG. 5. Comparison of the average shielding $\langle\sigma(\mathrm{Xe}_n(\mathrm{CH}_4)_m)\rangle$ with $\langle\sigma(\mathrm{Xe}_n\mathrm{Ar}_m)\rangle$, all in ppm.

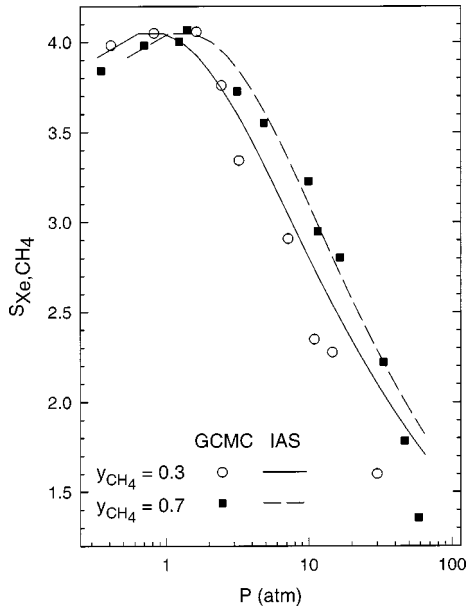

FIG. 6. The selectivity coefficients S_{XeCH_4} obtained from GCMC simulations are compared with the predictions of IAS theory from the adsorption isotherms of pure Xe and CH_4 at 300 K. The mole fractions of CH_4 in the gas phase are $y_{\mathrm{CH}_4}=0.7$(■) and $y_{\mathrm{CH}_4}=0.3$(○).

have been predicted from the internal volume of the cage and the known density dependence of the Xe chemical shift in the gas phase, since the one-body distribution function for Xe and the two-body distribution functions for Xe coadsorbate in the zeolite cage are distinctly different from the gas phase. Nevertheless, the observed (and calculated) chemical shift increments between Xe_n and $\mathrm{Xe}_n\mathrm{Kr}$ in zeolite Na*A* are found to be related to the observed increments between Xe_n and Xe_{n+1} (and to the calculated increments between Xe_n and $\mathrm{Xe}_n\mathrm{CH}_4$ or between Xe_n and $\mathrm{Xe}_n\mathrm{Ar}$) in the same way that the gas phase second virial coefficient of ^{129}Xe shielding for Xe–Kr (and Xe–CH_4 or Xe–Ar) is related to that for Xe–Xe. If we compare the increments in the chemical shifts of the Xe_n cluster upon addition of one Xe, or Kr, or CH_4, or Ar, we find that they are related in the same ratio as the second virial coefficients of the Xe chemical shift in the gas phase: That is, $\sigma_1(\mathrm{Xe}-\mathrm{Kr})/\sigma_1(\mathrm{Xe}-\mathrm{Xe})=0.53$ whereas the ratio of the increments range from 0.57 to 0.62. Similarly, $\sigma_1(\mathrm{Xe}-\mathrm{CH}_4)/\sigma_1(\mathrm{Xe}-\mathrm{Xe})=0.51$, whereas the ratio of increments range from 0.51 to 0.54; and $\sigma_1(\mathrm{Xe}-\mathrm{Ar})/\sigma_1(\mathrm{Xe}-\mathrm{Xe})=0.34$, whereas the ratio of increments range from 0.34 to 0.40. When the cages become crowded (more than 5 Xe atoms) the chemical shift increments no longer follow the gas phase trend. We expect the same relation for other sorbates (CO, CO_2, N_2) with Xe.

TABLE III. ^{129}Xe chemical shifts of the mixed clusters $\mathrm{Xe}_n\mathrm{CH}_4$ in the alpha cages of zeolite Na*A* (ppm relative to isolated Xe atom) compared with $\mathrm{Xe}_n\mathrm{Kr}$.

	$\delta(\mathrm{Xe}_n\mathrm{Kr})$			$\delta(\mathrm{Xe}_n\mathrm{CH}_4)$
Cluster	OBSD[a]	GCMC[b]	Cluster	GCMC[c]
$\mathrm{Xe}_1\mathrm{Kr}$	84.7	86.6	$\mathrm{Xe}_1\mathrm{CH}_4$	86.5
$\mathrm{Xe}_2\mathrm{Kr}$	103.3	101.5	$\mathrm{Xe}_2\mathrm{CH}_4$	102.6
$\mathrm{Xe}_3\mathrm{Kr}$	124.5	121.4	$\mathrm{Xe}_3\mathrm{CH}_4$	121.0
$\mathrm{Xe}_4\mathrm{Kr}$	148.9	144.6	$\mathrm{Xe}_4\mathrm{CH}_4$	143.3
$\mathrm{Xe}_5\mathrm{Kr}$	174.7	173.3	$\mathrm{Xe}_5\mathrm{CH}_4$	170.9
$\mathrm{Xe}_6\mathrm{Kr}$	209.9	208.6	$\mathrm{Xe}_6\mathrm{CH}_4$	204.4

[a]Reference 45.
[b]Reference 16.
[c]This work.

Selectivity coefficients for Xe and CH_4 *and ideal adsorbed solution theory*

First we consider the inside vs outside distribution of the sorbate molecules. This difference in composition between the adsorbed phase and the bulk phase in equilibrium with it is captured by a single quantity called the separation factor or selectivity coefficient. We use the conventional definition of selectivity as the ratio of the mole fractions in the zeolite to the ratio of the mole fractions in the bulk:[46,47]

$$S_{\mathrm{Xe,CH}_4}=\frac{x_{\mathrm{Xe}}/x_{\mathrm{CH}_4}}{y_{\mathrm{Xe}}/y_{\mathrm{CH}_4}} \quad \text{or} \quad \frac{\{\langle n\rangle_{\mathrm{Xe}}/\langle m\rangle_{\mathrm{CH}_4}\}}{\{\rho_{\mathrm{Xe}}/\rho_{\mathrm{CH}_4}\}}. \tag{13}$$

Theoretical separation factors may be obtained from the individual single-component adsorption isotherms if each component adsorbed independently of the other. In Fig. 6 we show the separation factors or selectivity coefficients from GCMC simulations compared with those calculated from the pure isotherms using ideal adsorbed solution (IAS) theory. We calculated the spreading pressure π, or rather $(\pi A/RT)$, by integration,

$$(\pi A/RT)=\int_0^p \langle n\rangle_{\mathrm{Xe}}(p)\,\frac{dp}{p} \tag{14}$$

for the pure components using the adsorption isotherms from the GCMC simulations of the pure Xe and pure CH_4 in zeolite Na*A*. Then from the plots of $(\pi A/RT)$ vs p we obtain at a given total pressure the mole fractions x_{Xe} and y_{Xe}.[46] The agreement of the IAS curves with the actual GCMC results (shown in Fig. 6) for mixtures of Xe and CH_4 in Na*A* at 300 K is reasonably good. IAS theory serves as a good guide as to what selectivity coefficients to expect. There is a preferred adsorption of Xe compared to CH_4 in Na*A*, somewhat similar to the Xe–Kr selectivity, not as pronounced as in Xe–Ar mixtures. We find that the ideal adsorbed solution model gives good predictions for $P<10$ atm, and starts to fail at higher pressures. The GCMC results show that the preferential adsorption of Xe is decreased somewhat by increasing the mole fraction of CH_4 in the bulk phase (good only for $P<1$ atm) or by increasing the total pressure (at any bulk composition). Figure 6 shows that at higher total pressures of Xe–CH_4 mixtures, GCMC simulations predict the CH_4 molecule becomes more competitive with the Xe than the ideal adsorbed solution predicts. This is consistent with our findings in simulations of Xe–Ar competitive adsorption. For the same mole fractions and total pressure in the bulk phase, the selectivity coefficients $S_{Xe,\,CH_4}$ (comparable to $S_{Xe,\,Kr}$) are not as large as $S_{Xe,\,Ar}$.[10]

Comparison of the GCMC results with the simple hypergeometric model

Next we consider distribution of the sorbate molecules among the cavities of the microporous solid. This can be expressed in terms of the fraction $f(n,m)$ of cages having n molecules of one type (Xe) and m molecules of the other type (CH_4) in a zeolite having an overall average number $\langle n\rangle_{Xe}$ and $\langle m\rangle_{CH_4}$ of molecules per cage. The $f(n,m)$ in the Xe–CH_4/Na*A* systhtem cannot be observed directly experimentally since the CH_4 molecules are freely exchanging among the cavities. However, we have directly measured P_n, the fraction of cages that have exactly n Xe atoms, with various numbers of CH_4 molecules. We can compare distributions obtained from the GCMC simulations with those from the simple model of a binary mixture in which the component molecules are distinguishable but equivalent in competition for a fixed number of lattice sites per cage under the rule of mutual exclusion, in which the distribution among cavities can be trivially obtained. The fraction of cages having n molecules of one type (Xe) and m molecules of the other type (CH_4) is given by

$$f(n,m)=H_i\langle n\rangle^n\langle m\rangle^m/\left\{n!m!\sum_{k=0}^{n}[\langle n\rangle^k\langle m\rangle^{i-k}/k!(i-k)!]\right\}, \qquad (15)$$

where H_i is given by the hypergeometric distribution, which in the limit of a large number of subvolumes (alpha cages) takes the form,[4]

$$H_i=\langle i\rangle^i(K-\langle i\rangle)^{(K-i)}K!/K^K i!(K-i)! \qquad (16)$$

where $\langle i\rangle=N/M=$ the average number of molecules per subvolume (N molecules in M alpha cages). In the case of xenon in the alpha cages of zeolite Na*A*, it can be assumed that $K=8$ is a reasonable model since no more than eight Xe atoms have been found in an alpha cage of Na*A*. We compared the $f(n,m)=$ from GCMC simulations with the predictions of Eq. (15) and found that the simple model works just as well for Xe–CH_4 mixtures as it does for Xe–Kr and better than for Xe–Ar mixtures in Na*A*.[16]

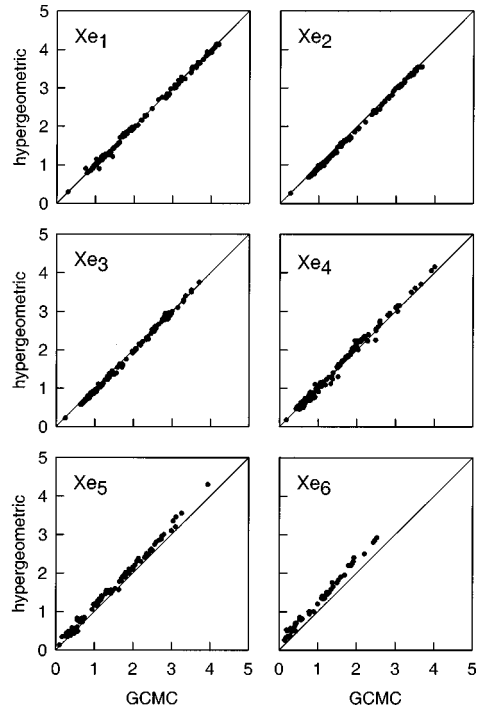

FIG. 7. The average number of CH_4 molecules in those cages having exactly n Xe atoms, $[\langle m\rangle_{CH_4}]_n$. The results from GCMC simulations for a wide range of overall $\langle n\rangle_{Xe}$ and $\langle m\rangle_{CH_4}$ are compared with results from the simple hypergeometric mixture model.

For any $\langle n\rangle$ and $\langle m\rangle$, the average number of CH_4 molecules in those cages having exactly n Xe atoms, $[\langle m\rangle_{CH_4}]_n$ is trivially obtained. These $[\langle m\rangle_{CH_4}]_n$ are compared with the GCMC results in Fig. 7 for Xe_1 to Xe_6. The simple hypergeometric mixture model gives results nearly indistinguishable from GCMC for the average number of CH_4 molecules in the same cavity as Xe_1, but has systematic deviations from the GCMC results for cavities containing Xe_2 to Xe_6, as seen in Fig. 7. The simple model gives larger average numbers of CH_4 molecules in the same cavity as Xe_5 and Xe_6 throughout the whole range of values of $[\langle m\rangle_{CH_4}]_n$ than does GCMC. The deviations shown here between the GCMC results and the simple hypergeometric model are responsible for the deviations between the chemical shifts observed experimentally, shown as points in Fig. 4, and the lines which are the average chemical shifts based on Xe and CH_4 distributions taken from the simple model.

For a fixed total number of Xe atoms in the zeolite, how are the CH_4 molecules distributed among cages with differing number of Xe atoms? $[\langle m\rangle_{CH_4}]_n$ decreases with increasing n, largest for those cages containing no Xe atoms and smallest for those cages containing seven Xe atoms. As the total number of CH_4 molecules is increased, each of the $[\langle m\rangle_{CH_4}]_n$ increases. This larger average number of CH_4

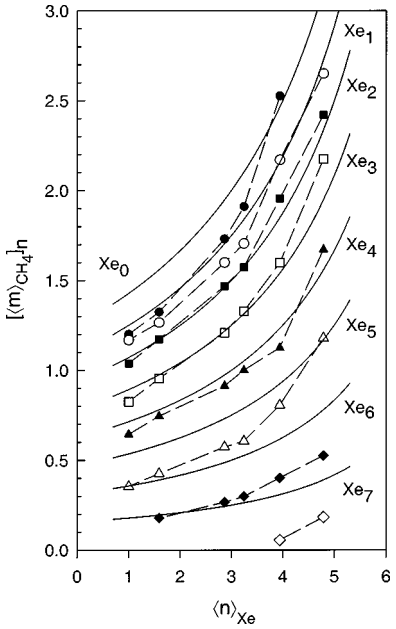

FIG. 8. For a fixed total number of CH_4 molecules in the zeolite, how are they distributed among cages with differing number of Xe atoms? The solid curves are the average number of CH_4 molecules in the same cage as the Xe_n cluster, $[\langle m\rangle_{CH_4}]_n$ vs overall $\langle n\rangle_{Xe}$ for fixed overall $\langle m\rangle_{CH_4}=1.250$, calculated from the hypergeometric distribution. The points are calculated from GCMC simulations.

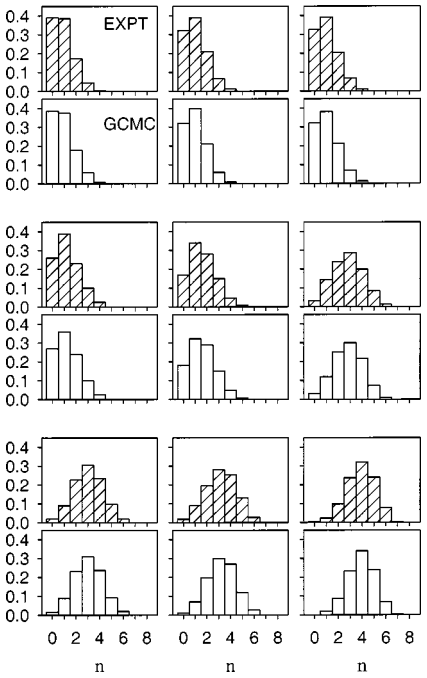

FIG. 9. The fractions of alpha cages containing n Xe atoms, P_n, from experiment and from GCMC simulations. The loadings are as follows. For the top row, $\langle n\rangle_{Xe}=0.888$, $\langle m\rangle_{CH_4}=1.509$ (GCMC): $\langle n\rangle_{Xe}=0.925$, $\langle m\rangle_{CH_4}=1.533$); 1.046, 3.860 (GCMC: 1.038, 3.850); 1.056, 2.208 (GCMC: 1.076, 2.253). For the middle row: $\langle n\rangle_{Xe}=1.250$, $\langle m\rangle_{CH_4}=0.915$ (GCMC: 1.246, 0.884); 1.593, 1.175 (GCMC: 1.592, 1.170); 2.780, 1.274 (GCMC 2.814, 1.353). For the bottom row: $\langle n\rangle_{Xe}=3.010$, $\langle m\rangle_{CH_4}=2.079$ (GCMC: 3.026, 2.016); 3.166, 1.179 (GCMC: 3.217, 1.182); 3.887, 0.681 (GCMC: 3.915, 0.703).

visitors in turn causes the chemical shift of every Xe_n peak to increase with increasing $\langle m\rangle_{CH_4}$, as is seen in Fig. 4. Because $[\langle m\rangle_{CH_4}]_n$ decreases with increasing n, there results a compression in the chemical shift differences between the Xe_n peaks with increasing overall $\langle m\rangle_{CH_4}$, to the point that at high enough CH_4 loading, the chemical shift differences of the Xe_n peaks can no longer be resolved, and only a broad single peak is observed. We can already see the trend toward that limit in the spectrum (d) in Fig. 3 of a sample having an average $\langle m\rangle_{CH_4}=3.86$ CH_4 molecules per cage.

For a fixed total number of CH_4 molecules, in the zeolite, how are the CH_4 molecules distributed among cages with differing number of Xe atoms? As already described above, $[\langle m\rangle_{CH_4}]_n$ generally decreases with increasing n, but what is the trend when samples with a low $\langle n\rangle_{Xe}$ are compared against samples with a higher $\langle n\rangle_{Xe}$? We find in the simple model and in the GCMC simulations that $[\langle m\rangle_{CH_4}]_n$ is larger for every Xe_n in the higher $\langle n\rangle_{Xe}$ samples. At low $\langle n\rangle_{Xe}$, say 1.00, the CH_4 molecules are distributed among cages having few Xe atoms, so there are many unoccupied lattice sites for CH_4 molecules to go into. At high loading of Xe, say $\langle n\rangle_{Xe}=5.00$, the same fixed number of CH_4 molecules will be distributed among cages containing many more Xe atoms. Since the total number of sites available for the fixed total number of CH_4 molecules decreases as the sites have been taken up by Xe atoms, $[\langle m\rangle_{CH_4}]_n$ for each Xe_n cluster is larger than in the low $\langle n\rangle_{Xe}$ sample. The simple model shows these general trends in the calculated distributions in Fig. 8 for a fixed overall $\langle m\rangle_{CH_4}=1.250$, predicting quite well the trend that the $[\langle m\rangle_{CH_4}]_n$ for each Xe_n cluster goes up as $\langle n\rangle_{Xe}$ increases in the results from GCMC simulations. As the $\langle n\rangle_{Xe}$ varies from 1.0 to 7.0 the total number of sites available for the fixed total number of CH_4 molecules decreases as the sites are taken up by Xe atoms which are increasing in total number. The consequence is that the $[\langle m\rangle_{CH_4}]_n$ for each Xe_n cluster goes up as $\langle n\rangle_{Xe}$ increases. This larger average number of CH_4 visitors in turn causes the chemical shift of the Xe_n peak to increase with increasing $\langle n\rangle_{Xe}$, the curious secondary effect seen experimentally in Fig. 4, where the filled circles lie at higher chemical shifts (larger negative shielding) than the open circles. Figure 8 predicts that this increase in the $[\langle m\rangle_{CH_4}]_n$ for a given Xe_n cluster as the overall $\langle n\rangle_{Xe}$ increases, is less and less pronounced with increasing n. There are consequences in the Xe_n chemical shifts; for example, comparing Xe_1 with Xe_4 in Fig. 4, we see that the gap between the filled circles and the open circles decreased.

Comparison of GCMC simulations with experiment

Distributions of xenon and CH_4

The experimental distributions, the fraction of cages containing n Xe atoms, and any number of CH_4 molecules, P_n, obtained from the intensities of the Xe_n peaks, are well reproduced by the GCMC simulations for all nine samples, as shown in Fig. 9. For a given xenon loading, the experimental P_n values in zeolite samples containing mixtures of Xe and CH_4 appear not to be systematically different from

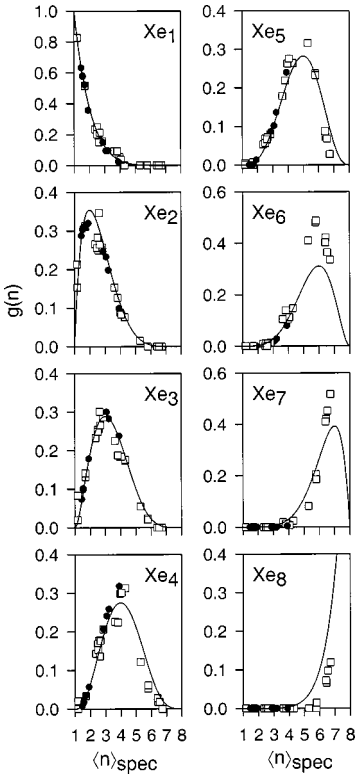

FIG. 10. Experimental equilibrium distribution of Xe atoms at 300 K among those cages occupied by Xe atoms. Shown are the fraction $g(n)$ of cages containing Xe_n in samples of zeolite Na*A* containing: (□) pure Xe and (●) a mixture of Xe and CH_4. $\langle n\rangle_{spec}$ of a sample is the average Xe occupancy of cages containing Xe, which can be obtained directly from the spectrum. The fractions predicted by the hypergeometric distribution for eight equivalent lattice sites is shown as the solid curve in each case.

the experimental P_n values in zeolite samples containing pure Xe. This is best illustrated by a comparison of the $g(n)$, that fraction of those cages occupied with Xe, that have exactly nXe atoms, shown in Fig. 10. The points are obtained directly from the experimental intensities of the Xe_n peaks in samples of pure Xe and of mixtures of Xe–CH_4 in Na*A*. The distribution of the Xe atoms among the cages ($g(n)$) appear not to be significantly different, whether the cages are partly occupied by CH_4 molecules or not. We found this to be the case for co-adsorbed Xe and Ar as well,[10] but this is probably not generally true. It is easy to imagine that for a fairly bulky coadsorbate that is not free to exchange from cage to cage, the Xe will find an effectively smaller cage where coadsorbates are present. In Fig. 10 the curves based on the simple hypergeometric model show systematic deviations from experiment. Results of GCMC simulations in pure Xe and in mixtures, not shown, completely overlap the experimental $g(n)$ values, showing the identical systematic deviations as the experiment from the simple model.

Finally, the distributions that we observe experimentally and find in GCMC simulations are not consistent with the 13 adsorbates per cage that are reported in other simulations.[48]

^{129}Xe chemical shifts

One of the interesting experimental observations is that the larger the Xe_n cluster the smaller the dependence of the

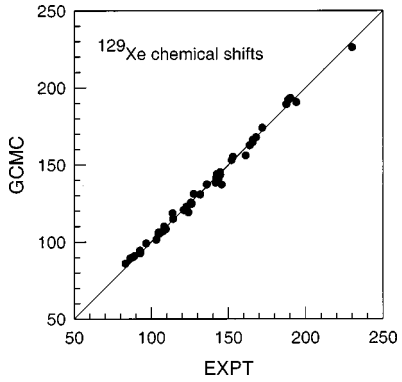

FIG. 11. The ^{129}Xe chemical shifts of Xe_n with CH_4 under fast exchange in zeolite Na*A*, predicted by GCMC simulations are compared with the experimental values for all nine samples. The shifts are in ppm relative to the isolated Xe atom.

^{129}Xe chemical shift on the overall $\langle m\rangle_{CH_4}$. This is observed despite the fact that the larger Xe_n clusters have larger incremental shifts. The explanation for this is an obvious one: Xe_1 can have any number from 1 to 9 CH_4 molecules with it in the cage, and the Xe_1 chemical shift can thus vary over a wide range, according to the $[\langle m\rangle_{CH_4}]_1$ for the cages containing only one Xe atom, as the overall $\langle m\rangle_{CH_4}$ is varied. On the other hand, Xe_7 can have at most 1 or 2 CH_4 molecules with it in the cage, no matter how much the overall $\langle m\rangle_{CH_4}$ is increased. The Xe_n chemical shift trends are fully explained by the simple hypergeometric mixture model, since the $[\langle m\rangle_{CH_4}]_n$ determine the incremental shift of the Xe_n peak as the overall loading of CH_4 increases, and the secondary effect leads to smaller or larger incremental shifts for lower or higher $\langle n\rangle_{Xe}$. We demonstrate this in Fig. 4, where the average shielding of each mixed cluster $Xe_n(CH_4)_m$ obtained from GCMC are used and the distributions are calculated entirely according to the simple model. We find that the qualitative trends in the experimental chemical shifts (points) are well reproduced by these calculations (lines). Thus, a strictly statistical model for the distribution of binary mixtures among the cavities is sufficient to explain the trends in the chemical shift increments. However, deviations from simple model distributions start to affect the accuracy of representation of experimental results for clusters Xe_3 or larger. And of course, we needed the GCMC simulations to obtain the proper average shieldings of the mixed clusters $Xe_n(CH_4)_m$ that are used in the calculations for the lines in Fig. 4.

How well do the GCMC simulations reproduce the observed chemical shifts in all nine Xe–CH_4/Na*A* samples? In Fig. 11 the total intermolecular chemical shift measured relative to the isolated Xe atom, the ^{129}Xe chemical shift for Xe_n in an alpha cage with an average number of CH_4 molecules under fast exchange (which is directly calculated in the GCMC simulations) is plotted in comparison with the experimental values also measured relative to the isolated Xe atom. We see in Fig. 11 that in an absolute measure, the chemical shifts that we calculate are in good agreement with experiment. This ability to reproduce the chemical shifts of all the peaks in all the samples implies that the GCMC simu-

lations provide a reasonably accurate representation of both the distribution of CH_4 molecules among the cavities containing Xe atoms and the distribution of configurations of each mixed $Xe_n(CH_4)_m$ cluster within one cavity sampled at room temperature.

CONCLUSIONS

We have investigated the $Xe-CH_4$ mixture in zeolite Na*A* as a model system for competitive adsorption in microporous solids. The Xe_n clusters are trapped in the alpha cages of this zeolite for times sufficiently long that it is possible to observe individual peaks in the NMR spectrum for each cluster while the CH_4 molecules are in fast exchange between the cages and also with the gas outside. The ^{129}Xe NMR spectra of nine samples of varying Xe and CH_4 loadings provide detailed information in the form of ^{129}Xe chemical shifts and the intensities of the peaks which are dependent on the average methane and xenon occupancies. It has been possible to determine experimentally the average number of molecules of the second sorbate occupying the same cage as n atoms of the first sorbate. Grand canonical Monte Carlo simulations of mixtures of Xe and CH_4 in a rigid zeolite Na*A* lattice provide the detailed distributions and the average cluster shifts, as well as the distributions P_n, the fraction of cages containing n Xe atoms regardless of the number of CH_4 molecules. The agreement with experiment is reasonably good for all nine samples. The absolute chemical shifts for all the Xe_n peaks observed at 300 K in the nine samples, spanning a 200 ppm range, are well reproduced by the GCMC simulations. Although the detailed distributions, $f[Xe_n(CH_4)_m]$, the fractions of cages containing specifically n Xe atoms and m CH_4 molecules, have not been observed directly in this system, this information is contained both in the observed ^{129}Xe chemical shifts of the Xe_n peaks and in the observed distributions P_n. Therefore, these two types of observables provide critical tests for computer simulations of $f[Xe_n(CH_4)_m]$.

In a strictly statistical model of a binary mixture in which the component molecules are distinguishable but equivalent in competition for eight lattice sites per cage under mutual exclusion, a hypergeometric distribution, the distribution among cavities $f[Xe_n(CH_4)_m]$ can be trivially obtained. This simple model therefore provides a limiting case against which both the GCMC simulations and the experimental $Xe-CH_4$ system may be compared. This model is found to be very helpful in understanding the experimental observations. The strictly statistical components of the observed trends in the distributions and the ^{129}Xe chemical shifts of the Xe_n peaks can be determined separately, and these can be treated in the limiting case of an ideal mixture. Deviations from the ideal mixture behavior are then separately examined, providing additional insight.

The present study provides a paradigm for investigations of coadsorption in zeolites over a wide range of loadings. In this particular system, and indeed in any other system in which the Xe has long residence times while the coadsorbate is fast exchanging between cages, the intensity of each Xe_n peak provides a quantitative measure of the distributions of the two types of sorbates among the cages, and the ^{129}Xe chemical shift of the Xe_n peak provides a measure of their distributions within a cage. These distributions, for a very broad range of overhead pressures and mole fractions of the bulk gas, are not available from any other experiments.

ACKNOWLEDGMENTS

This research has been supported by the National Science Foundation (Grant No. CHF95-28066) and by the University of Illinois Foundation through a Senior University Scholar Award to C.J.J.

[1] *Zeolites and Related Microporous Materials: State of the Art 1994*, edited by J. Weitkamp, H. G. Karge, H. Pfeiffer, and W. Hölderich (Elsevier, Amsterdam, 1994), Part IV, Diffusion and Adsorption, pp. 1133–1371.
[2] D. M. Ruthven, AIChE. J. **22**, 753 (1976).
[3] B. F. Chmelka *et al.*, Phys. Rev. Lett. **66**, 580 (1991); **67**, 931 (1991).
[4] C. J. Jameson, A. K. Jameson, R. Gerald II, and A. C. de Dios, J. Chem. Phys. **96**, 1676 (1992).
[5] R. G. Larsen *et al.*, Chem. Phys. Lett. **214**, 220 (1993).
[6] A. K. Jameson, C. J. Jameson, and R. E. Gerald II, J. Chem. Phys. **101**, 1775 (1994).
[7] C. J. Jameson, A. K. Jameson, R. E. Gerald II, and H.-M. Lim, J. Chem. Phys. **103**, 8811 (1995).
[8] I. Moudrakovski, C. I. Ratcliffe, and J. A. Ripmeester, J. Am. Chem. Soc. **120**, 3123 (1998).
[9] C. J. Jameson, A. K. Jameson, B. I. Baello, and H. M. Lim, J. Chem. Phys. **100**, 5965 (1994).
[10] C. J. Jameson, A. K. Jameson, and H. M. Lim, J. Chem. Phys. **104**, 1709 (1996).
[11] C. J. Jameson and H. M. Lim, J. Chem. Phys. **107**, 4373 (1997).
[12] M. P. Allen and D. J. Tildesley, *Computer Simulation of Liquids* (Clarendon, Oxford, 1987).
[13] J. J. Pluth and J. V. Smith, J. Am. Chem. Soc. **102**, 4704 (1980).
[14] G. E. Norman and V. S. Filinov, High Temp. **7**, 216 (1969).
[15] G. B. Woods, Ph.D. thesis, Oxford University, 1989.
[16] C. J. Jameson, A. K. Jameson, and H. M. Lim, J. Chem. Phys. **107**, 4364 (1997).
[17] R. A. Aziz and M. J. Slaman, Mol. Phys. **57**, 825 (1986).
[18] G. C. Maitland, M. Rigby, E. B. Smith, and W. A. Wakeham, *Intermolecular Forces, Their Origin and Determination* (Clarendon, Oxford, 1981).
[19] C. J. Jameson, A. K. Jameson, R. E. Gerald II, and H. M. Lim, J. Phys. Chem. **101**, 8418 (1997).
[20] R. Righini, K. Maki, and M. L. Klein, Chem. Phys. Lett. **80**, 301 (1981).
[21] N. Meinander and G. C. Tabisz, J. Chem. Phys. **79**, 416 (1983).
[22] S. Murad and K. E. Gubbins, in *Computer Modeling of Matter*, ACS Symposium Series 86, edited by P. Lykos (American Chemical Society, Washington, DC, 1978), p. 62.
[23] J. B. Nicholas *et al.*, J. Phys. Chem. **97**, 4149 (1993).
[24] G. Liuti, F. Pirani, U. Buck, and B. Schmidt, Chem. Phys. **126**, 1 (1988).
[25] J. Brewer, Technical Report AADD 663448, AFOSR No. 67-2795, Air Force Office of Scientific Research, Arlington, Virginia, 1967.
[26] A. E. Hansen and T. D. Bouman, J. Chem. Phys. **82**, 5035 (1985).
[27] K. Wolinski, J. Hinton, and P. Pulay, J. Am. Chem. Soc. **112**, 8251 (1990).
[28] H. H. Landolt and R. Börnstein, *Zahlenwerte und Funktionen*, 6 Auflage, Band I (Springer-Verlag, Berlin, 1950), Teil 1 (p. 401); Teil 3 (p. 511).
[29] *Ionization Potentials, Appearance Potentials, and Heats of Formation of Gaseous Positive Ions*, NSRDS-NBS 26 (National Bureau of Standards, Washington, DC, 1969).
[30] C. J. Jameson and H. S. Gutowsky, J. Chem. Phys. **40**, 1714 (1964).
[31] U. Buck, J. Schleusener, D. J. Malik, and D. Secrest, J. Chem. Phys. **74**, 1707 (1981).
[32] C. J. Jameson, A. K. Jameson, and S. M. Cohen, J. Chem. Phys. **65**, 3401 (1976).
[33] C. J. Jameson and A. C. de Dios, J. Chem. Phys. **97**, 417 (1992).
[34] C. J. Jameson, H. M. Lim, and A. K. Jameson, Solid State Nucl. Magn. Reson. **9**, 277 (1997).
[35] G. B. Woods and J. S. Rowlinson, J. Chem. Soc., Faraday Trans. 2 **85**, 765 (1989).

[36] M. W. Maddox, Ph.D. thesis, Oxford University, 1993.
[37] M. W. Maddox and J. S. Rowlinson, J. Chem. Soc., Faraday Trans. **9**, 3619 (1993).
[38] R. L. June, A. T. Bell, and D. N. Theodorou, J. Phys. Chem. **94**, 8232 (1990).
[39] A. V. Kiselev and P. Q. Du, J. Chem. Soc., Faraday Trans. 2 **77**, 17 (1981).
[40] E. Cohen de Lara and R. Kahn, J. Phys. (Paris) **42**, 1029 (1981).
[41] A. G. Bezus, M. Kočiřík, and E. A. Vasilyeva, Zeolites **7**, 327 (1987).
[42] F. Vigne-Maeder and A. Auroux, J. Phys. Chem. **94**, 316 (1990).
[43] H. Yucel and D. M. Ruthven, J. Chem. Soc., Faraday Trans. 1 **76**, 60 (1980).
[44] R. J. Harper, G. R. Stifel, and R. B. Anderson, Can. J. Chem. **47**, 4661 (1969).
[45] A. K. Jameson *et al.*, Solid State Nucl. Magn. Reson. **4**, 1 (1995).
[46] A. L. Myers and J. M. Prausnitz, AIChE. J. **11**, 121 (1965).
[47] D. M. Ruthven, *Principles of Adsorption and Adsorption Processes* (Wiley, New York, 1984).
[48] P. R. Van Tassel, H. T. Davis, and A. V. McCormick, Langmuir **10**, 1257 (1994).